Frontiers in Bioscience Landmark

Front. Biosci. (Landmark Ed) **2023**; 28(1): 9
https://doi.org/10.31083/j.fbl2801009

Original Research

Comprehensive Analysis of RNA-Binding Protein-Related lncRNA in Breast Invasive Carcinoma

Jiawei Zhou[1,2,†], Hui Zhao[3,†], Yugang Guo[1], Kaiqi Hou[1,4], Qian Ding[1], Wei Shao[1], Qian Xu[1,3,*]

[1]Henan Provincial Engineering Laboratory of Insects Bio-reactor, Nanyang Normal University, 473061 Nanyang, Henan, China
[2]School of Pharmacy, Hangzhou Normal University, 311121 Hangzhou, Zhejiang, China
[3]Zhengzhou Revogene Ltd., 451162 Zhengzhou, Henan, China
[4]Henan Engineering Research Center of Intelligent Processing for Big Data of Digital Image, School of Computer Science and Technology, Nanyang Normal University, 473061 Nanyang, Henan, China
*Correspondence: xuqian7666@nynu.edu.cn (Qian Xu)
[†]These authors contributed equally.
Academic Editor: Ricardo Jorge Pinto Araujo
Submitted: 13 August 2022 Revised: 16 November 2022 Accepted: 29 November 2022 Published: 13 January 2023

Abstract

Background: RNA-binding proteins (RBPs), which form complexes or single/multiple RNA-binding domains, have a functional role in regulating and determining the function or stability of the bound RNAs in various cancers, including breast invasive carcinoma (BRCA). However, the biological functions and clinical implications of RBP-related long noncoding RNAs (lncRNAs) in BRCA remain largely unknown. **Methods**: Herein, we first identified and characterized RBP-related lncRNAs in BRCA. Then we built an RBP-related lncRNA signature (RBPLSig) and explored the clinical evaluation and prediction performance of the RBPLSig by bioinformatic analysis. In addition, to optimize treatment plans, prediction online tools was developed to predict the patient survival rate. Lastly, to verify the function of lncRNA WAC antisense RNA 1 (*WAC-AS1*), the experiments such as Quantitative real-time PCR (qRT-PCR), lncRNA knockdown, CCK-8, and terminal deoxynucleotidyl transferase-mediated dUTP nick-end labeling (TUNEL) staining were performed. We also gained the potential mechanisms of the druggable compounds of the *WAC-AS1* related RBP gene, putative NSUN6, using molecular docking. **Results**: The results showed that RBPLSig, as an independent prognostic factor for BRCA patients, was involved in numerous malignancy-associated immunoregulatory pathways. We found different immune statuses and responses to immunotherapy, chemotherapy, and targeted therapy between the high- and low-risk groups stratified by RBPLSig. **Conclusions**: Our data broaden the comprehensive understanding of the biological functions of RBP-related lncRNAs, and demonstrate a novel and independent RBPLSig to assess prognosis and the immune microenvironment, thus helping to guide treatment decisions for BRCA.

Keywords: invasive breast carcinoma; RNA-binding proteins; long non-coding RNA; prognosis; tumor immune microenvironment

1. Introduction

Breast carcinoma is a leading cause of death worldwide, accounting for 684,996 (6.9%) deaths globally in 2020 (Cancer Today-IARC, 2020), despite dramatic advances in diagnosis and treatment strategies [1,2]. It is thus necessary to discover novel biomarkers for early diagnosis and therapeutic interventions. Long noncoding RNAs (lncRNAs) are a series of transcripts longer than 200 nucleotides that have limited protein coding capability [3–5]. Several studies have reported that the deregulation of lncRNAs, such as LncRNA *RP11-400K9.4* [6], lncRNA *DILA1* [7], and LncRNA *OIP5-AS1* [8] affects the tumorigenesis and progression of breast invasive carcinoma (BRCA). However, the detailed mechanism underlying the regulation and alteration of these lncRNAs in BRCA over time remains unknown.

To date, more than 1500 RNA-binding proteins (RBPs) have been identified [9]. Studies have shown that several RBPs are abnormally expressed in tumors and regulate various biological functions, including coordinating RNA splicing, nuclear export, transcript stabilization, localization, and degradation of all types of RNAs [10]. Considering the important role of RBPs in transcriptional and post-transcriptional gene expression, it is not surprising that aberrantly regulated RBPs participate in the progression of human diseases, including cancers [11].

Recent studies have indicated that several cancer-associated lncRNAs act via transcriptional regulation and post-transcriptional regulation mediated by well-known RBPs [12]. For example, human antigen R (HuR)-regulated lncRNA *NEAT1* is stabilized by HuR and functions as an oncogene in ovarian cancer [13]. LncRNA-*HGBC* is also stabilized by HuR and functions as an oncogene in gallbladder cancer [14]. HuR promotes the degradation of *HOTAIR* [15] by recruiting *let7-Ago2* in breast cancer. Moreover, both the nuclear export and mitochondrial localization of lncRNA-*RMRP* are modulated by HuR and G-rich RNA sequence binding factor 1 (*GRSF1*) [16]. However, more direct evidence of the correlations and concordant

links among RBPs, lncRNAs, and BRCA are needed to explore the potential of lncRNAs for future cancer diagnostic, therapeutic, or prognostic purposes. While immunotherapy is a promising remedial modality for BRCA treatment, the objective response rates to immune checkpoint inhibitor (ICI) blockade have remained low; notwithstanding, blocking ICIs is a widely used strategy in immunotherapy [17]. Therefore, it is critical to find a reliable biomarker that can be used to precisely screen BRCA patients for immunotherapy.

The aim of our study was to perform a comprehensive analysis of RNA-binding protein-related lncRNA in BRCA. We first explored the relationship between the expression of the RBP-related lncRNA signature (RBPLSig) and clinicopathological features. Then, for predicting the performance of the RBPLSig, a nomogram for BRCA and one nomogram for BRCA subtypes (luminal A and TNBC) were established, respectively. The latter is more appropriate for immunotherapy evaluation. In addition, to optimize treatment plans, prediction online tools was developed to predict the patient survival rate. Lastly, to verify the function of *WAC-AS1*, pathway enrichment, CCK-8, TUNEL, drug sensitivity, and molecular docking analyses were performed. These findings may increase our understanding of RBP-related lncRNAs in patients with BRCA.

2. Materials and Methods

2.1 Datasets and Sample Extraction

RNA-sequencing data, updated clinical data, and sample information of breast invasive cancer (BRCA) cohort were downloaded from the TCGA data portal (https://tcga-data.nci.nih.gov/tcga/) and 107 patients in GSE58812 for external validation was obtained from the Gene Expression Omnibus (GEO; https://www.ncbi.nlm.nih.gov/geo/) database. Patients who fulfilled the following selection criteria: (1) diagnosed with histologically confirmed BRCA; (2) available RNA-seq data; (3) available follow up were eligible for study enrollment. Finally, 1054 patients from TCGA-BRCA, 107 patients from GSE58812 were included for further analysis. For TCGA-BRCA data analysis, the established RNA matrix file was merged with Ref-Seq and used for all subsequent RNA-seq expression analyses. For the data from GEO datasets, the probe ID for each gene was converted to a gene symbols. All raw data were analysed using the 'limma' package in R (version 4.2.1, http://www.bioconductor.org/).

2.2 Identification of Prognostic RBP-Related lncRNAs and Construction of the RBPLSig Prognostic Model

In the current study, we established 1542 encoding RNA-binding proteins (RBPs) [9]. Correlations between lncRNAs and RBPs were calculated using Pearson's correlation coefficient using the limma R package [18]. A lncRNA with a correlation coefficient $|R^2| > 0.3$ and $p < 0.001$ was considered to be an RBP-related lncRNA. An RBPLSig was established based on a linear combination of the regression coefficient derived from the multivariate Cox regression model coefficients (β) and expression levels of the RBP-related lncRNAs. To calculated the risk score, the following formula was used: $\sum_{i=1}^{n} \beta i * (\text{expression of lncRNA})$ .Using the median score of the RBPLSig, patients were divided into high- or low- groups. Survival curves analysis was performed between high- or low- groups by using the "survival" and "survminer" packages. Besides, the receiver operating characteristic (ROC) analysis was performed by using the "timeROC" and "survivalROC" R packages to assess the prognostic accuracy of RBPLSig value. The distribution of patients with different risk scores was investigated by principal components analysis (PCA) using the R package "princomp", and the PCA 3D graph were visualized using the R packages "caterplot3D". The co-expression network and Sankey diagram were used to established and visualized the correlation between the poor prognostic RBP-related-lncRNAs in the prognostic model and their co-expressed RBP mRNAs.

2.3 Gene Set Enrichment Analysis (GSEA) and Principal Components Analysis (PCA)

To better research and further explore the molecular mechanisms underlying the prognostic difference between high- and low-risk groups the biological function of GSEA was performed to by using the GSEA tools (http://www.broadinstitute.org/gsea) [19]. Significant predefined biological processes and pathways were enriched with |normalized enrichment score (NES)| >1, false discover rate (FDR) <0.25, and $p < 0.05$, after performing 1000 permutations. In addition, the R package "plyr", "ggplot2", "grid" and "gridExtra" in R software was used to summarize the results of the Kyoto Encyclopaedia of Genes and Genomes (KEGG) pathway analysis. The reference file was downloaded from the Molecular Signatures Database (MSigDB) [20].

2.4 Clinical Evaluation and Prediction Performance of the RBPLSig

The univariate and multivariate Cox regression analyses were conducted with Cox proportional hazard regression models to analyze predictive independent factors. Then, a nomogram that included all independent factors predicting overal survival (OS) was developed using R version 4.0.3 (http://www.r-project.org/) with rms packages.

The immune cell infiltration level of each BRCA sample was quantified using CIBERSORT (http://cibersort.stanford.edu/). The relationship between RBPLSig and immune checkpoint inhibitor (ICI) gene expression was determined using the ggstatsplot package and violin plot visualization. To clinically evaluate the model for breast cancer treatment, we calculated the IC_{50} of therapeutic antitumor drugs, such as lapatinib, gemcitabine, paclitaxel, sunitinib, and tipifarnib, which are recommended for BRCA

treatment by AJCC guidelines. The difference in the IC_{50} between the high- and low-risk groups was compared by a Wilcoxon signed-rank test, and the results are shown as box drawings obtained using pRRophetic and ggplot2 of R. In addition, the consistency between the actual survival and the nomogram was evaluated using calibration curves to predict survival probability. The better the fit between the predicted calibration curve and the standard curve, the better the conformity of the prediction model.

2.5 Cell Culture, lncRNA Knockdown and qRT-PCR Analysis

Triple-negative breast cancer (TNBC) cell lines, MDA-MB-231 and HST578T cells, were obtained American Type Culture Collection (ATCC, Manassas, VA, USA) and cultured in DMEM (Gibco, Waltham, MA, USA), containing 4500 mg/L glucose and 10% fetal bovine serum in 5% CO_2 conditions at 37 °C. To verify the function of *WAC-AS1*, specific siRNA (Guangzhou RiboBio Co., Ltd, Guangzhou, China) was designed and synthesized against it. TRIzol Reagent (Invitrogen, Carlsbad, CA, USA) was used to extract total RNA from two TNBC cell lines; subsequently, the iScript cDNA synthesis kit (Forma Scientific, Marietta, OH, USA) was used to generate cDNA. Real-time PCR was then performed with SYBR Green Real-time PCR Master Mixes (Thermo Fisher Scientific, Waltham, MA, USA) on a CFX96 Real-time PCR Detection System (Bio-Rad, Hercules, CA, USA). Data were normalized to *GAPDH* as an internal control, and results were analyzed as previously described [21].

2.6 Cell Survival and Apoptosis Assays

The Cell Counting Kit-8 (CCK-8) assay was used to examine the survival of TNBC cells following the protocol of the CCK-8 assay kit (Dojindo, Kyushu, Japan). Survival rates of the two TNBC cell lines after si-*WAC-AS1* knockdown was measured at 450 nm [22]. Cellular apoptosis was quantified via terminal deoxynucleotidyl transferase-mediated dUTP nick-end labeling (TUNEL) staining following the protocol of the One Step TUNEL Apoptosis Assay Kit (Keygen, Nanjing, China) [22]. The treated TUNEL-positive TNBC cells were counted under a fluorescence microscope (Olympus, Tokyo, Japan).

2.7 Drug Sensitivity Analysis in BRCA Cell Lines

We used the cell miner interface (https://discover.nci.nih.gov/cellminer/), containing 727 FDA-approved drugs and clinical trial drugs along with their corresponding protein targets in 60 cancer cell lines, to download the DTP NCI-60 database and RNA-seq data. Then, Spearman or Pearson correlation were used to analyze the association between RBP gene (*NSUN6*) expression and drug treatment response in five BRCA cell lines.

2.8 Molecular Docking Technology

The 2D structure of the drug molecules was searched using PubChem (https://pubchem.ncbi.nlm.nih.gov/), and a mol2 file was converted using Chem3D (PerkinElmer, Waltham, MA, USA). Receptor proteins were searched from the Protein Data Bank (http://www.rcsb.org/). Dehydration and ligand elimination were performed using PyMOL software (PyMOL2.3, https://pymol.org). The docking site was set in a cubic box in the center of the initial ligand, and a grid map of each atom type in the box was computed. The AutoDockTools 1.5.6 software (https://autodocksuite.scripps.edu/adt/) was used to simulate the molecular docking of potential targets and components. The best scoring conformer of each compound was analyzed and visualized in AutoDockTools-1.5.6 and PYMOL. Concurrently, we used Gromos96 (G43A1, http://gromos.net/) for dynamic simulation, which was performed for 10 ns in combination with the Extended Simple Point Charge (SPCE) water model [23]. System stability was evaluated by the root-mean-square deviation (RMSD) method.

2.9 Statistical Analysis

Statistical analyses were conducted using the R software V4.2.1 (http://www.bioconductor.org/) and SPSS V18.0 (IBM Corp., Armonk, NY, USA). The Kaplan–Meier method was used for survival analysis. The statistical analysis of clinical information was performed using a chi-square test or Fisher's exact test. The statistical significance of the difference between two groups was assessed using a Student's *t*-test, and $p < 0.05$ was considered statistically significant.

3. Results

3.1 Identification of RBP-Related lncRNAs with Significant Prognostic Value in BRCA

We first screened 1542 RBP-related encoding genes (mRNAs) and identified the available expression data of 1550 total lncRNAs as RBP-related lncRNAs in the TCGA-BRCA set ($|R^2| > 0.3$, $p < 0.001$). Among the lncRNAs selected, 61 had prognostic value for patients with BRCA through univariate Cox regression ($p < 0.05$, **Supplementary Table 1**). Next, 20 prognostic RBP-related lncRNAs were identified as poor prognostic factors though multivariate Cox proportional hazards regression analysis, including *MAPT-AS1*, *AL138724.1*, *AC004585.1*, *LINC00667*, *LINC01871*, *AL359752.1*, *AP003469.4*, *AL122010.1*, *AC061992.1*, *AL357054.4*, *LINC00987*, *SEMA3B-AS1*, *WAC-AS1*, *AL136368.1*, *AL136531.1*, *USP30-AS1*, *Z68871.1*, *AC245297.3*, *AC009119.1*, and *AP003119.3*. **Supplementary Fig. 1A** shows the co-expression network of six lncRNAs (*AC004585.1*, *AP003469.4*, *WAC-AS1*, *Z68871.1*, *AC009119.1*, and *AP003119.3*) and related RBPs. These lncRNAs were identified as poor prognostic factors because HR (hazard ratio) >1. The Sankey diagram show the co-expression

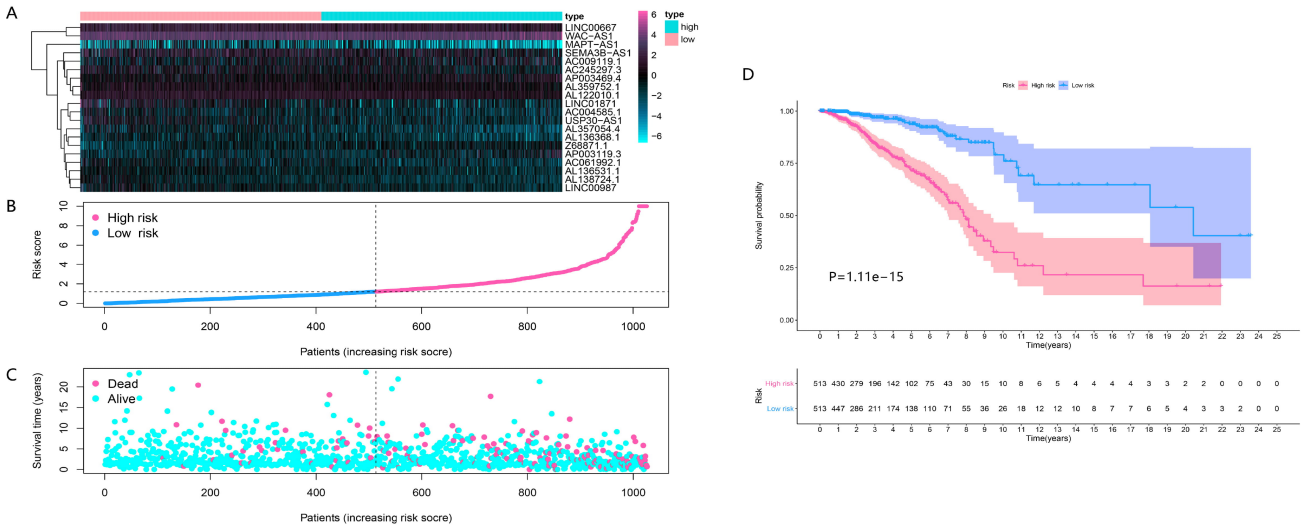

Fig. 1. The prognostic value of the RBPLSig. (A) Heatmap demonstrating the expression levels of 20 prognostic lncRNAs between the high- and low-risk groups. (B,C) Hierarchical clustering analysis of survival status of patients with increased risk score. (D) Kaplan–Meier analysis of the prognostic model in TCGA-BRCA.

relationship between RBPs genes and related prognostic lncRNAs **Supplementary Fig. 1B**).

3.2 Construction of a Prognostic RBP-Related lncRNA Signature

After multivariate Cox proportional hazards regression analysis, the 20 lncRNAs were used to establish a prognostic RBP-related lncRNA signature (RBPLSig). The estimated RBPLSig was calculated as follows: = (–0.258 × *MAPT-AS1*$_{\text{expression}}$) + (–0.312 × *AL138724.1*$_{\text{expression}}$) + (0.248 × *AC004585.1*$_{\text{expression}}$) + (–0.109 × *LINC00667*$_{\text{expression}}$) + (–0.265 × *LINC01871*$_{\text{expression}}$) + (–0.166 × *AL359752.1*$_{\text{expression}}$) + (0.105 × *AP003469.4*$_{\text{expression}}$) + (–0.193 × *AL122010.1*$_{\text{expression}}$) + (–0.231 × *AC061992.1*$_{\text{expression}}$) + (–0.249 × *AL357054.4*$_{\text{expression}}$) + (–0.159 × *LINC00987*$_{\text{expression}}$) + (–0.061 × *SEMA3B-AS1*$_{\text{expression}}$) + (0.060 × *WAC-AS1*$_{\text{expression}}$) + (–0.382 × *AL136368.1*$_{\text{expression}}$) + (–0.320 × *AL136531.1*$_{\text{expression}}$) + (–0.181 × *USP30-AS1*$_{\text{expression}}$) + (0.529 × *Z68871.1*$_{\text{expression}}$) + (–0.109 × *AC245297.3*$_{\text{expression}}$) + (0.046 × *AC009119.1*$_{\text{expression}}$) + (0.049 × *AP003119.3*$_{\text{expression}}$). Using the median risk score as the threshold, the risk score of each patient was calculated, after which patients were divided into low- and high-risk groups (Fig. 1). Notably, patient mortality risk increased with an increasing risk score, and the expression of 20 lncRNAs in the RBPLSig was associated with the risk score (Fig. 1A–C). Kaplan–Meier survival curves showed a significant difference in OS between the high-RBPLSig and low-RBPLSig groups for patients with BRCA ($p < 0.0001$, Fig. 1D), suggesting that the patients with low-risk scores had a greater chance of achieving the same survival time than the high-risk score group (Fig. 1D).

3.3 Evaluation and Validation of the RBPLSig as an Independent Prognostic Factor for BRCA Patients

Univariate and multivariate Cox regression analyses were performed to determine whether the RBPLSig is an independent prognostic factor for BRCA. The hazard ratio (HR) of the risk score was 1.104 (95% confidence interval [CI] 1.081–1.128, $p < 0.001$) in the univariate Cox regression analysis (Fig. 2A) and 1.078 (95% CI 1.052–1.104, $p < 0.001$) in the multivariate Cox regression analysis (Fig. 2B). The area under the curve (AUC) values of multiple clinicopathological factors such as age, stage, and Classification of Malignant Tumors (TNM) stage, were significantly different between the two groups stratified by RBPLSig (Fig. 2C). The risk score showed a relatively higher AUC value with respect to multiple clinicopathological factors for the TCGA-BRCA cohort (5-year: 0.777, 8-year: 0.8, 10-year: 0.811, and 15-year: 0.804, Fig. 2D) and validation cohort (GSE58812) (3-year: 0.682, 5-year: 0.719, 8-year: 0.663, and 10-year: 0.657, Fig. 2E). PCA further verified that the RBPLSig was a risk factor related to prognosis, with moderate sensitivity and specificity. The high- and low-risk groups could not be effectively discriminated using the whole genome or RBP-related lncRNAs; however, using RBPLSig, the high- and low-risk patients could be clearly distinguished, further supporting the accuracy of the model. These results indicated that RBPLSig is a significant independent prognostic risk factor for patients with BRCA (Fig. 2F–H).

3.4 Correlation between RBPLSig and Clinicopathological Factors

To further assess whether the 20 RBP-related lncRNAs participated in the development of BRCA, the relationship between the risk score and clinicopathological factors

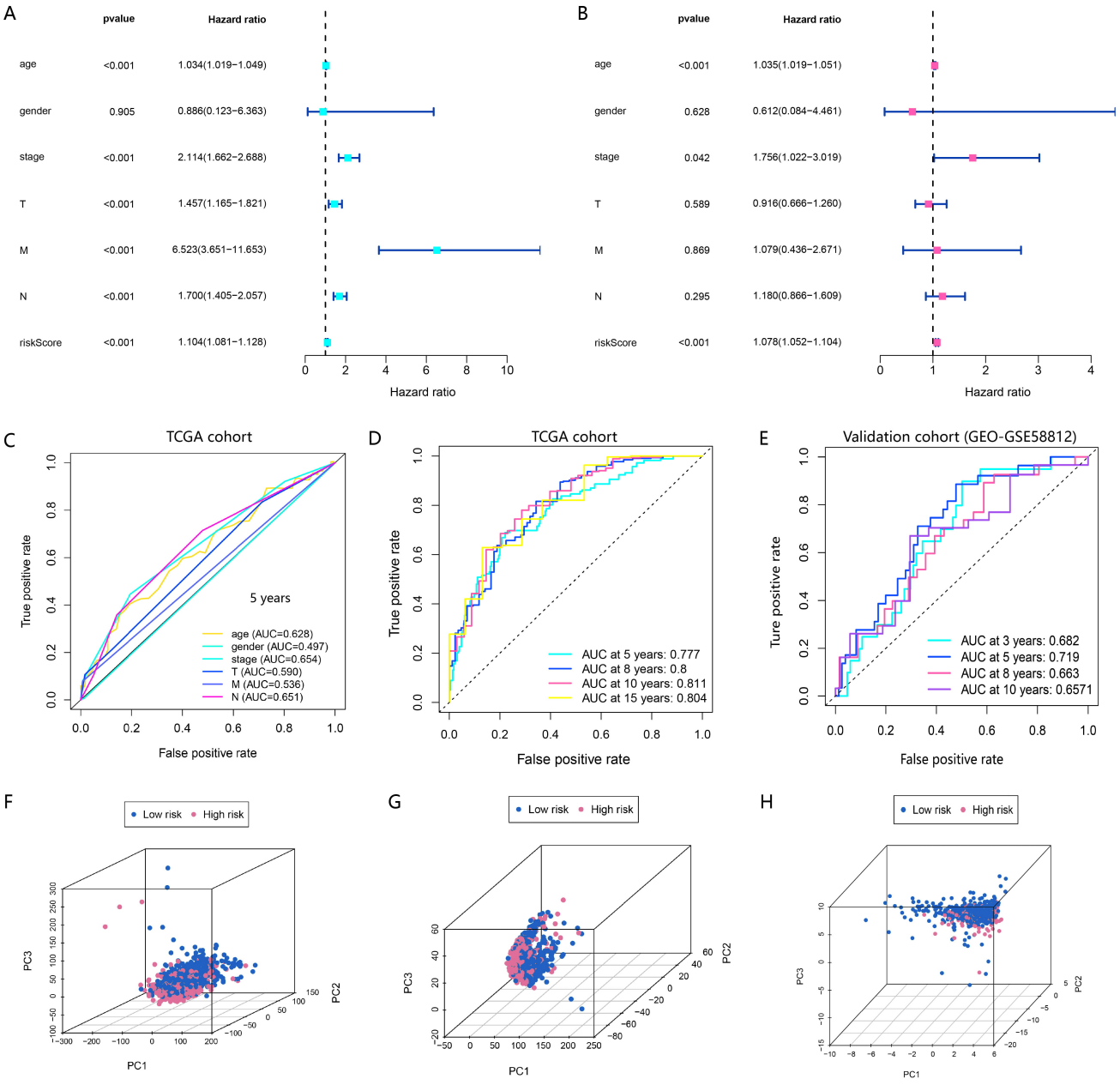

Fig. 2. The RBPLSig is an independent prognostic factor for OS prediction. (A,B) Univariate and multivariate Cox regression analyses to screen OS-related factors. (C) Receiver operating characteristic (ROC) curve analysis of clinicopathological features. (D) Time-dependent ROC curves of OS at 5-, 8-,10- and 15-years in TCGA-BRCA cohort. Their AUC values are all greater than 0.75. The closer the AUC is to 1.0, the higher the authenticity of the detection method. (E) Time-dependent ROC curves of OS at 3-, 5-, 8- and 10-years in the validation cohort. Their AUC values are all greater than 0.65. (F–H) Principal component analysis (PCA) of the high- and low-risk groups based on the whole-genome (F), RBP-related lncRNAs (G), and RBPLSig expression profiles (H).

was analyzed. As shown in Fig. 3A–E, an association was found between the risk score and clinicopathological factors ($p < 0.001$). Apparently, patients with low-risk scores were clustered more in luminal A and triple negative breast cancer (TNBC) subtypes, whereas patients with high-risk scores were clustered more in HER2-enriched and luminal B subtypes (Fig. 3F, $p < 0.001$).

3.5 Bioinformatics Analysis between the Two Groups Stratified by RBPLSig

GSEA was performed to further examine RBPLSig-associated signaling pathways in BRCA. We observed that transforming growth factor β signaling pathways were enriched in the high-risk group. Meanwhile, as shown in Fig. 4A and **Supplementary Table 2**, several immuno-related signaling pathways, such as B cell receptor, T cell receptor, natural killer (NK) cell-mediated

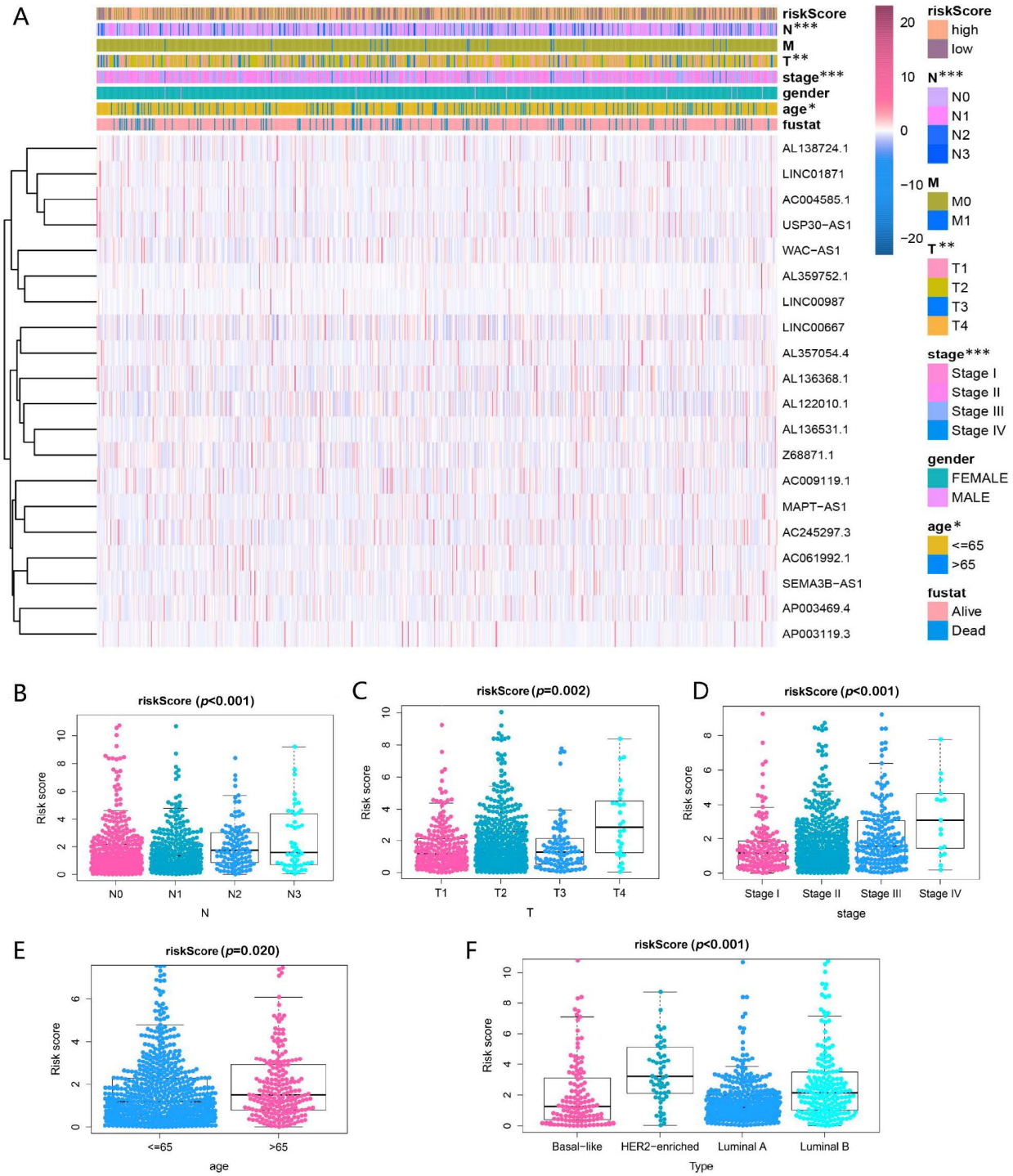

Fig. 3. Prognostic risk score associated with the clinical characteristics of patients with BRCA. (A) Heatmap and clinicopathologic features of high- and low-risk groups. *$p < 0.05$, **$p < 0.01$, and ***$p < 0.001$. (B–F) Distribution of risk scores stratified by (B) N-stage ($p < 0.001$), (C) T-stage ($p < 0.01$), (D) stage ($p < 0.001$), (E) age ($p < 0.05$) and (F) tumor subtypes ($p < 0.001$).

cytotoxicity, and the vascular endothelial growth factor (*VEGF*) signaling pathway were enriched in the low-risk group. Further, among the lncRNAs selected in RBPLSig, six of these 20 lncRNAs (*USP30-AS1*, *AC004585.1*, *AC009119.1*, *AL138724.1*, *LINC00987* and *LINC01871*) (**Supplementary Fig. 2**) were associated with lymph node metastasis. Additionally, 18 of 20 lncRNAs in RBPLSig (*AL136368.1*, *AL136531.1*, *AL138724.1*, *LINC01871*, *MAPT-AS1*, *AL357054.4*, *AC061992.1*, *AL122010.1*, *USP30-AS1*, *AL359752.1*, *LINC00987*, *AC245297.3*, *LINC00667*, *SEMA3B-AS1*, *AP003119.3*, *WAC-AS1*, *AC004585.1* and *Z68871.1*) were associated with immune subtypes (Fig. 4B, $p < 0.05$). These results indicate that RBPLSig and RBPLSig-associated

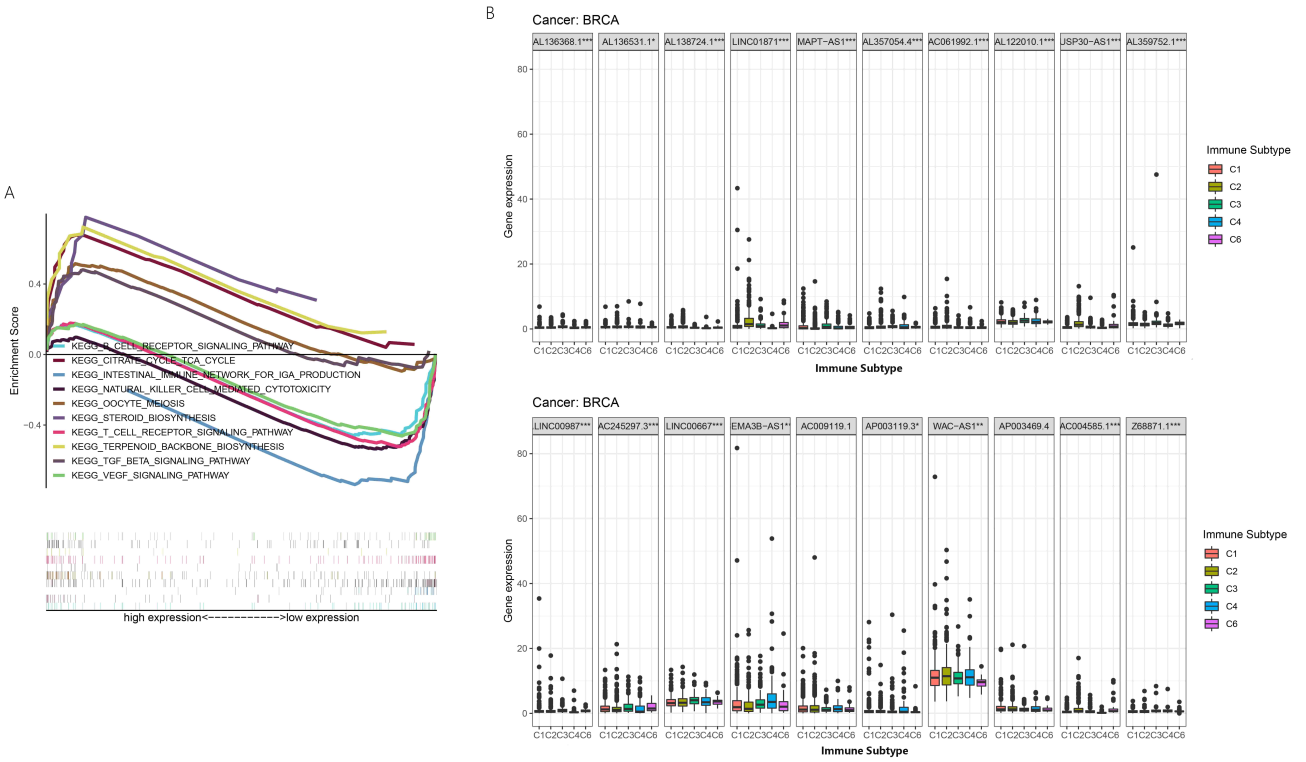

Fig. 4. Bioinformatics analysis between the two groups stratified by RBPLSig. (A) GSEA for biological pathways and processes correlated with immune score values in the cohort from TCGA. (B) Association of 20 lncRNAs expression with different immune infiltrate subtypes tested with ANOVA (analysis of variance) in TCGA-BRCA. ns, not significant; *$p < 0.05$; **$p < 0.01$; ***$p < 0.001$. C1: wound healing, C2: INF-r dominant, C3: inflammatory, C4: lymphocyte depleted, C5: immunologically quiet, and C6: TGF-β-dominant.

lncRNAs may participate in tumor progression and the tumor immune microenvironment (TIME). In addition, we analyzed the correlation between 20 lncRNAs and stromal score. The expression level of *WAC-AS1*, *LINC01871*, *AC004585.1*, *SEMA3B-AS1*, *AL136531.1*, *AP003119.3*, *AL136368.1*, *USP30-AS1* and *LINC00987* in BRCA patients demonstrated a significant correlation with stromal score ($p < 0.05$), especially *AC004585.1* and *LINC00987* ($r > 0.4$) (**Supplementary Fig. 3**). We also found that eight out of 20 lncRNAs were associated with immune score, and 11 out of 20 lncRNAs were associated with tumor purity (Estimate score) (**Supplementary Fig. 3**).

3.6 Immune Status and Response to Clinical Treatment between the Two Groups Stratified by RBPLSig

To evaluate the correlation between the risk score and tumor immune cell infiltration, the CIBERSORT algorithm was used to investigate the scale of 22 immune cell types. Patients with high-risk scores had higher macrophage M0 and macrophage M2 infiltration levels than those with low-risk scores ($p \leq 0.001$). In contrast, patients with low-risk scores had higher ratios of B cell-naive, plasma cells, T cells CD8, T cells CD4 memory activated, T cells regulatory, NK cell activated, dendritic cells resting, and neutrophils (Fig. 5A, $p \leq 0.05$). This indicates that patients with different immune status patterns in different groups could be classified by the RBPLSig.

Expression of the ICI (immune checkpoint inhibitor) genes and/or their ligands have attracted widespread attention as BRCA biomarkers for immune checkpoint blockade therapy. It is critically important to effectively screen BRCA patients who might benefit most from different ICI immunotherapies. To further investigate the association between risk score and ICIs, cytotoxic T-lymphocyte-associated antigen 4 (*CTLA-4*), sialic acid binding Ig-like lectin 15 (*Siglec-15*), programmed cell death-1 (*PD-1*), and programmed cell death-ligand 1 (*PD-L1*) were selected to compare the expression patterns between the two groups stratified by the RBPLSig. The result indicates that patients in the low-risk group tended to have higher *PD1*, *PD-L1*, and *CTLA-4* expression levels than those in the high-risk group, whereas patients in the high-risk group tended to have higher *Siglec-15* expression levels (Fig. 5B, $p < 0.05$). These results further indicate that the RBPLSig may serve as a potential predictive biomarker for treatment responses to ICI immunotherapy. We validated the RBPLSig for 12 cancer types suitable for immunotherapy to determine whether it could be effectively used as a prognostic signature for other cancer types. Interestingly, of the 12 cancer types, RBPLSig was negatively correlated with the

Table 1. The prognosis efficiency of RBPLSig for 12 types of cancers suitable for immunotherapy.

Cancer types	Over survival	High risk	Low risk	AUC		
	(*p*-value)	(n)	(n)	1-year	3-year	5-year
BLCA	<0.0001	202	202	0.648	0.687	0.714
CESC	<0.0001	145	146	0.7	0.737	0.726
COAD	<0.0001	182	182	0.718	0.74	0.743
KIRC	<0.0001	263	263	0.713	0.704	0.739
KIRP	<0.0001	143	143	0.868	0.824	0.8
LAML	<0.0001	65	65	0.779	0.783	0.796
LUAD	<0.0001	254	255	0.65	0.616	0.664
LUSC	=0.086	249	250	0.574	0.58	0.594
OV	<0.0001	188	188	0.636	0.65	0.703
PAAD	<0.0001	88	88	0.673	0.798	0.95
READ	=0.017	78	79	0.665	0.715	0.879
SKCM	<0.0001	231	232	0.699	0.704	0.7

BLCA, Bladder Urothelial Carcinoma; CESC, Cervical squamous cell carcinoma and endocervical adenocarcinoma; COAD, Colon adenocarcinoma; KIRC, Kidney renal clear cell carcinoma; KIRP, Kidney renal papillary cell carcinoma; LAML, Acute myeloid leukemia; LUAD, Lung adenocarcinoma; LUSC, Lung squamous cell carcinoma; OV, Ovarian serous cystadenocarcinoma; PAAD, Pancreatic adenocarcinoma; READ, Rectum adenocarcinoma; SKCM, Skin Cutaneous Melanoma.

prognosis of 11 cancer types, while the AUCs corresponding to the 1-, 3-, and 5-year survival for five cancers (CESC: cervical squamous cell carcinoma and endocervical adenocarcinoma; COAD: colon adenocarcinoma; KIRC: kidney renal clear cell carcinoma; KIRP: kidney renal papillary cell carcinoma and LAML: acute myeloid leukemia) were higher than 0.7 (Table 1). In addition to immune checkpoint blockade therapy, the associations between the risk score and the efficacy of targeted therapeutics and chemotherapeutics in treating patients with BRCA were then identified. The low-risk group had a higher IC_{50} for lapatinib ($p < 0.001$). However, the high-risk group had a higher IC_{50} for gemcitabine, paclitaxel, sunitinib, and tipifarnib ($p < 0.001$). Collectively, this suggests that the RBPLSig may be a sensitive predictor of drug sensitivity (Fig. 5C).

3.7 Construction of Predictive Nomograms and Online Analysis Tools

To generate a clinically applicable model for individual OS prediction, we first constructed a nomogram that accurately estimates the 5-, 8-, 10-, and 15-year survival probabilities in BRCA patients using the RBPLSig and other clinicopathological independent prognostic factors (Fig. 6A). The calibration curves of the nomogram for predicting patient survival at 5-,8-,10-, and 15-years are shown in Fig. 6B–E. Considering that (1) the risk score was lower for luminal A and TNBC than for HER2-enriched and luminal B subtypes, and (2) patients with a low-risk score had an improved TIME (appropriate for immunotherapy), we further constructed a nomogram for BRCA subtypes (luminal A and TNBC) appropriate for immunotherapy evaluation (**Supplementary Fig. 4**). To further explore the value of predictive nomograms, we developed an online analysis tools to predict the survival rate and recommended medication for BRCA patients (https://www.origingenetic.com/BreastCancerModel). With the aid of the prediction online tools, clinicians can assist in evaluating patient survival rates to optimize treatment plans.

3.8 WAC-AS1 Silencing Induces TNBC Cell Apoptosis

For further study on the potential function of these lncRNAs and to verify the aforementioned results, we focused on the upregulated *WAC-AS1*, which is associated with metastasis and poor prognosis for OS in selective patient subgroups from TCGA and Gene Expression Omnibus (GEO) datasets (Fig. 7A–C).

Next, we synthesized a specific smart RNA silencer (including small interfering RNA and small nucleolar RNAs) against *WAC-AS1*. The RT-qPCR indicates that smart RNA silencer-*WAC-AS1* (si-*WAC-AS1*) could abolish the expression of *WAC-AS1* in TNBC cell lines (MDA-MB-231 and HST578T cells; Fig. 7D). The CCK-8 assay indicates that cell viability was diminished by silencer-*WAC-AS1* transfection compared to that with si-NT (Fig. 7E,F, $p < 0.05$). The TUNEL assay was in line with the CCK-8 assay data and demonstrated that MDA-MB-231 and HST578T cell apoptosis could be enhanced by si-*WAC-AS1* transfection compared to that with si-NT (Fig. 7G, $p < 0.05$). Finally, in the pathway analysis, different malignancy-associated pathways were enriched in different groups based on *WAC-AS1* (Fig. 7H,I and **Supplementary Table 3**).

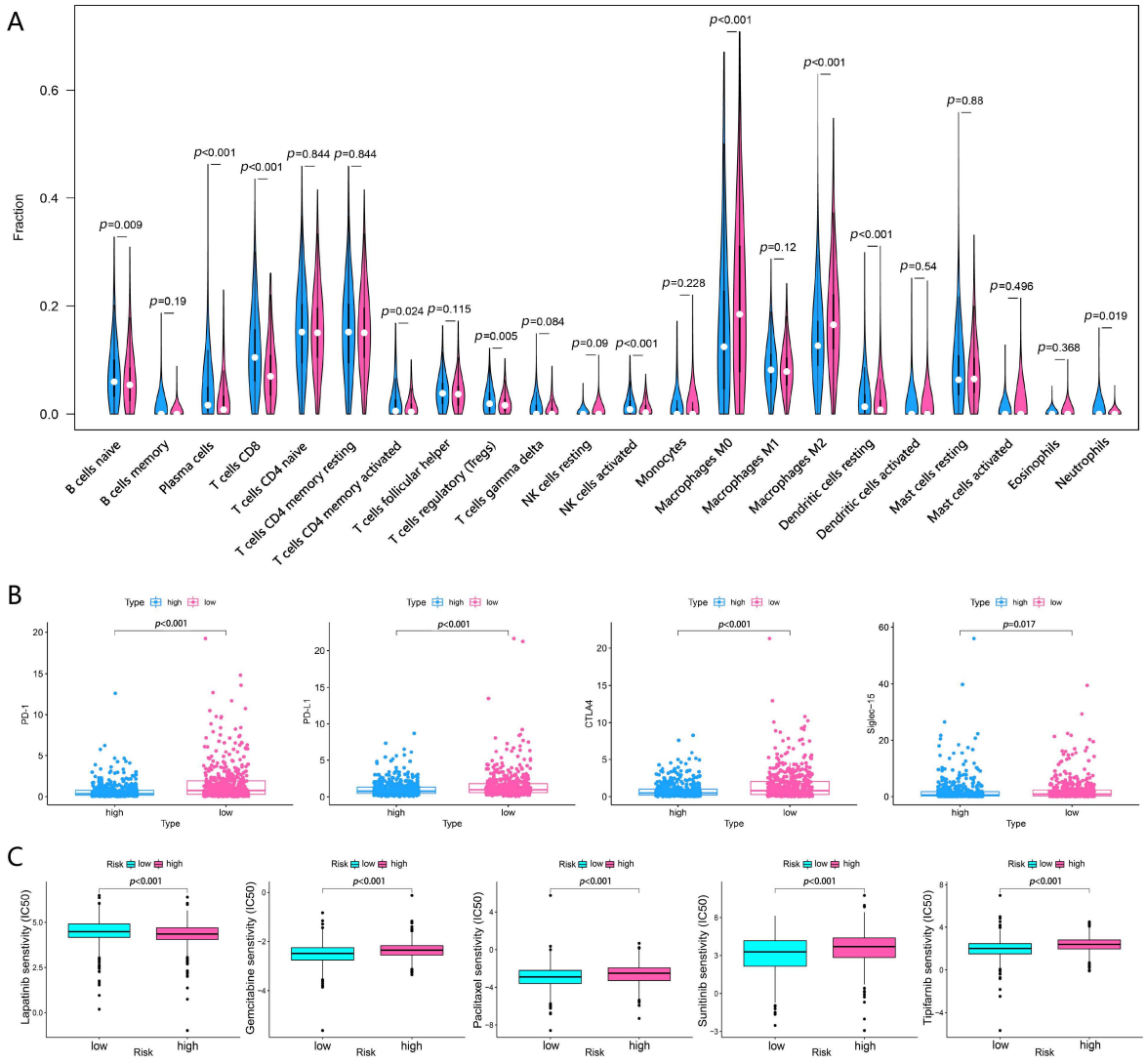

Fig. 5. Different responses to immunotherapy, chemotherapy and targeted therapy between the two groups stratified by RBPLSig. (A) Violin plot of 22 immune-related terms were incorporated to assess the abundance of immune cells between the two groups stratified by RBPLSig, in which red represents the high-risk samples, and blue the low-risk samples. (B) The expression of *PD-1* ($p < 0.001$), *PD-L1* ($p < 0.001$), *CTLA-4* ($p < 0.001$) and *Siglec-15* ($p < 0.05$) between the low- and high-risk groups in the cohort from TCGA. (C) Five drugs include lapatinib ($p < 0.001$), gemcitabine ($p < 0.001$), paclitaxel ($p < 0.001$), sunitinib ($p < 0.001$) and tipifarnib ($p < 0.001$) susceptibility distribution between the high and low risk groups.

3.9 Prediction of Drug Sensitivity in BRCA Cell Lines and Molecular Docking Technology

Currently, lncRNAs are usually used as prognostic or diagnostic biomarkers and lncRNA-based drug targets [24], the latter of which, while reported in several studies, still requires more research [25]. Accordingly, the search for new lncRNA-based drugs is considered a promising field. Targeting the binding partners (pro-oncogenic RBPs) may indirectly affect the function of these related pro-oncogenic lncRNAs. Drug sensitivity analysis was performed on five breast cancer cell lines, including MCF7, MDA-MB-231, HS 578T, BT-549, and T-47D ($|r| \geq 0.9$, $p < 0.001$). Strikingly, after further screening, NOP2/Sun RNA methyltransferase 6 (NSUN6; PDBID: 5WWQ), which was co-expressed with the pro-oncogenic lncRNA *WAC-AS1* (cor = 0.37, $p < 0.001$), was associated with sensitivity to navitoclax in five BRCA cell lines (cor = 0.996, $p < 0.001$, **Supplementary Fig. 5**). We gained mechanical insights into the potential mechanisms of the druggable compounds of an RBP gene, putative NSUN6, using molecular docking. The crystal structure of the RBP gene, mainly protease, was collected from the PDB database (http://www.rcsb.org/structure/NSUN6) with PDB ID 5WWQ, for docking analysis with navitoclax (Fig. 8). The active cavity box parameter setting center_x, y, z was 54.315, 33.779 and 135.063, respectively, while size_x, y, z was 92, 64, 108, whereas amino acid residues were within 3.4Å around the active site. The minimum docking affinity between navito-

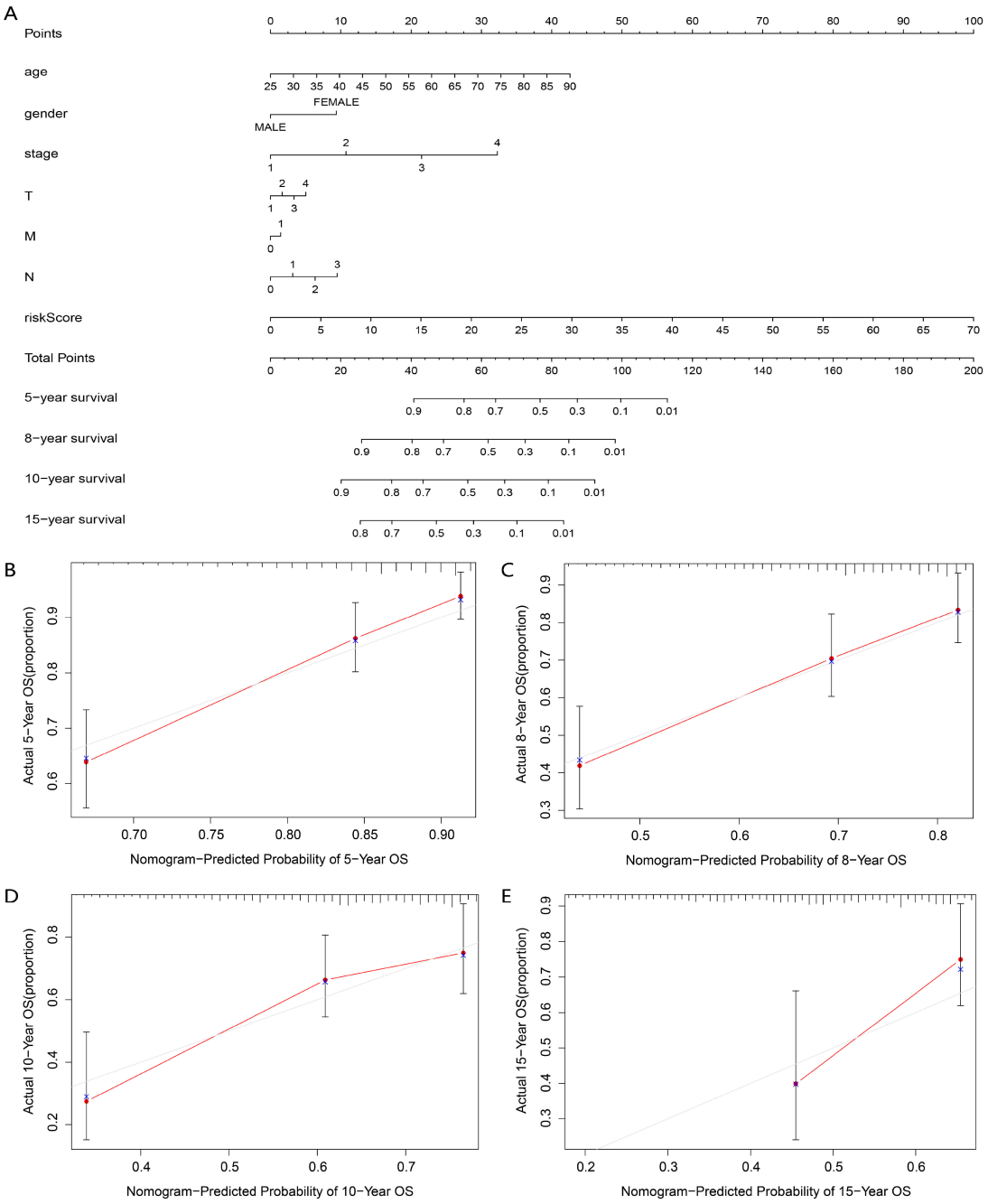

Fig. 6. Construction of a nomogram for survival prediction. (A) The clinical prognostic nomogram developed to predict 5-, 8-, 10-, and 15-year survival. (B–E) Calibration curves showing nomogram predictions for (B) 5-, (C) 8-, (D) 10- and (E) 15-year survival.

clax and NSUN6 is –9.0 (kcal/mol). The lower the docking score (the greater the negative value), the higher the binding force is between the compound and the protein. The bond action showed that navitoclax forms a hydrogen bond with the residue of six amino acids (SER-210, SER-207, TYR-131, ARG-197, GLN-78, and GLU-74) of NSUN6(RBP) (Fig. 8A), suggesting that navitoclax has a good binding activity with the NSUN6 protein. Next, the behavior of NSUN6, associated with navitoclax sensitivity in a simulative aquatic ecosystem, was analyzed. After a 10 ns simulation, the root-mean-square deviation (RMSD) tended to be flat; the display system reached equilibrium. Although the structure and conformation of the ligand changed, the complex did not separate, and the ligand receptor was tightly bound in the target region, indicating that the site changed to be a possible target (Fig. 8B,C). Taken together, these predictions indicate that navitoclax may be a useful treatment option for TNBC patients with high expression of the pro-oncogenic NSUN6 and the binding partner lncRNAs. Although preliminary, this study presents compelling data for the design of lncRNA-based drugs; it is hoped that future studies will expand upon our themes.

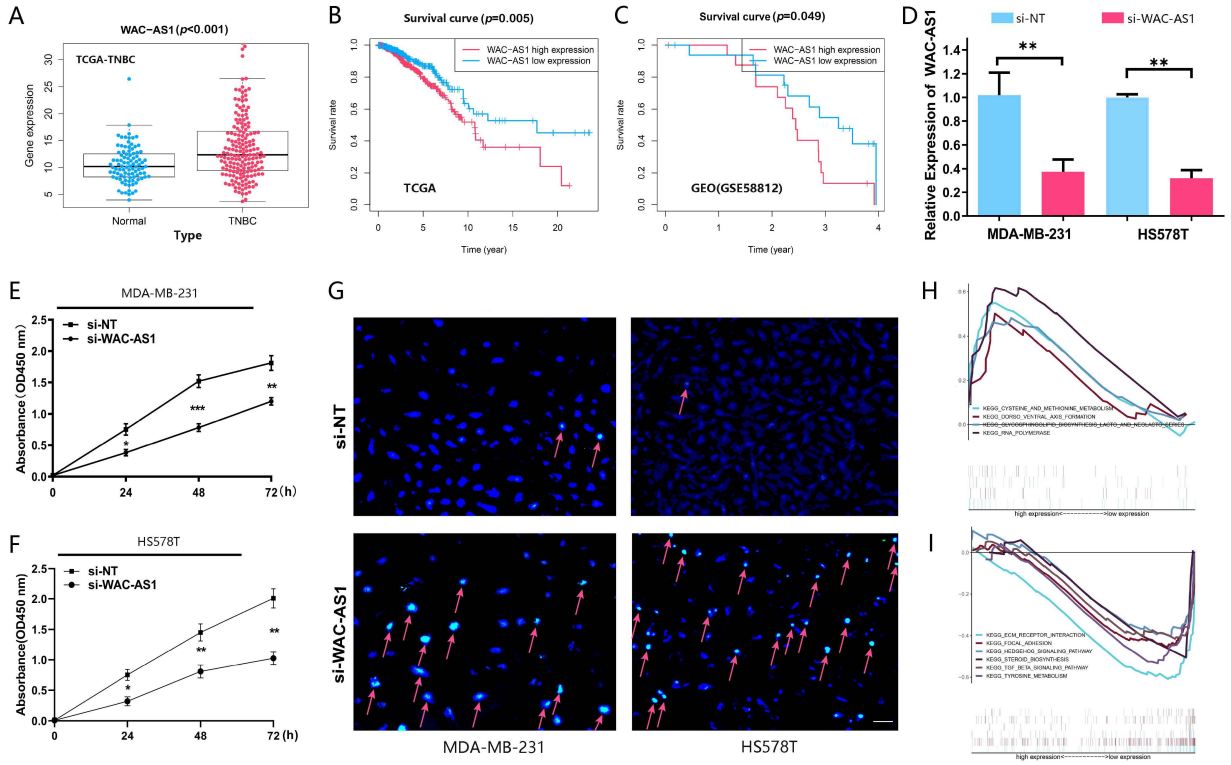

Fig. 7. *WAC-AS1* was upregulated in TNBC tissues and *WAC-AS1* silencing induced TNBC cells apoptosis. (A) Microarray analysis of *WAC-AS1* in TCGA-TNBC tissues corresponding normal tissues. (B,C) Kaplan-Meier survival curves of patients with different level of *WAC-AS1* in TCGA (B) and GEO (C) datasets. (D) TNBC cell lines (MDA-MB-231and HS578T) was transfected with si-*WAC-AS1*. The expression of *WAC-AS1* in TNBC cell lines was analyzed by qRT-PCR. (E–G) The Effects of si-*WAC-AS1* on the proliferation and apoptosis of TNBC cell lines was detected by CCK-8 assay (E,F) and TUNEL assay (G). * $p < 0.05$, ** $p < 0.01$ compared with si-NT group. (H,I) GSEA was used to analyze the signaling pathways enrichment in different groups.

4. Discussion

Several studies have revealed that the aberrant expression of lncRNAs is a key regulator of many cellular processes. The specificity of these processes, which contribute to carcinogenesis and tumor progression, may greatly depend on their protein interactors, including classical RBPs and unconventional RBPs [26]. RNA functions greatly depend on RNA-protein interactors, including those with RBPs. In particular, several emerging RBPs are well recognized in regulating lncRNA stability, transport, and localization [27]. Some RBP-related lncRNAs in the RBPLSig have been reported to be beneficial prognostic indicators in BRCA. However, many questions about how RBP-related lncRNAs affect the occurrence and development of BRCA remain to be elucidated.

Among the 20 RBP-related lncRNAs (*AL136368.1*, *AL136531.1*, *AL138724.1*, *LINC01871*, *MAPT-AS1*, *AL357054.4*, *AC061992.1*, *AL122010.1*, *USP30-AS1*, *AL359752.1*, *LINC00987*, *AC245297.3*, *LINC00667*, *SEMA3B-AS1*, *AC009119.1*, *AP003119.3*, *WAC-AS1*, *AP003469.4*, *AC004585.1*, and *Z68871.1*), 14 were associated with a good prognosis, whereas six were associated with a poor prognosis. *MAPT-AS1*, *LINC00667*, and *SEMA3B-AS1* have been confirmed to play roles in the pathogenesis and prognosis of various cancer types. For example, high expression of *MAPT-AS1* is associated with better survival rates in patients with BRCA [28]. *LINC00667* has been reported to be responsible for non-small cell lung cancer [29] and colorectal cancer progression [30]. Consistently, overexpression of oncogenic *SEMA3B-AS1* is associated with poor survival outcomes in hepatocellular carcinoma and gastric cancer [31,32]. Furthermore, recent studies revealed that seven RBP-related lncRNAs *(LINC01871* [33], *AC061992.1* [34], *AL122010.1* [35], *USP30-AS1* [36], *Z68871.1* [33,35], *AC245297.3* [35], and *AP003119.3* [35]) included in the RBPLSig could be prognostic factors in some cancers. Nevertheless, the biological functions and the underlying molecular mechanisms of these lncRNAs in cancer have not yet been clarified. The prognostic roles of the remaining 10 lncRNAs (*AL136368.1*, *AL136531.1*, *AL138724.1*, *AL357054.4*, *AL359752.1*, *LINC00987*, *AC009119.1*, *WAC-AS1*, *AP003469.4*, and *AC004585.1*) in cancers have not been previously reported. We further used *in vitro* experiments to initially validate the results, focusing on the expression, prognostic value, and associated pathways

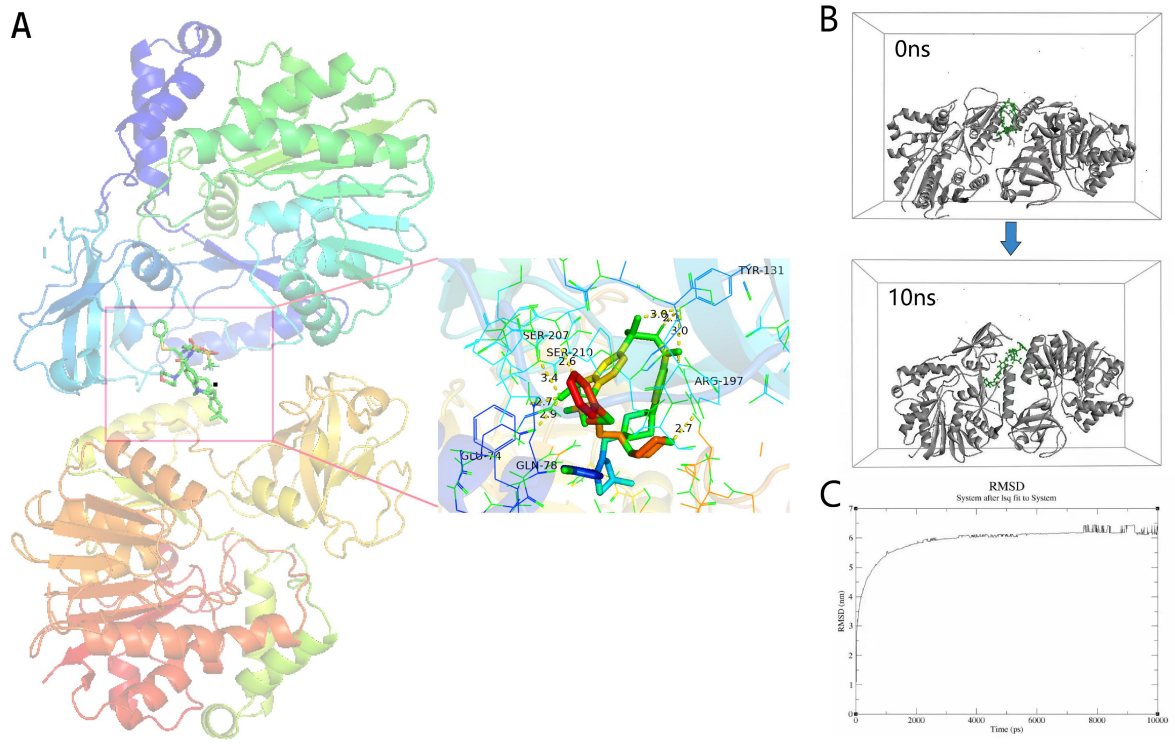

Fig. 8. Molecular docking analysis. (A) Molecular docking results of navitoclax-NSUN6 (NOP2/Sun RNA methyltransferase 6 NSUN6; PDBID: 5WWQ). Hydrogen bonds are shown as yellow dotted lines. (B) Snapshots of navitoclax-NSUN6 system after 10 ns. (C) RMSD of navitoclax-NSUN6 systems. RBP, RNA-binding protein.

of the lncRNA *WAC-AS1* in selective TNBC patient subgroups from TCGA-TNBC and GEO datasets. We then conducted an *in vitro* experiment using TNBC cell lines. The results demonstrated that lncRNA *WAC-AS1* silencing induced TNBC cell apoptosis.

In studies of lncRNA functions, it is important to determine how many such lncRNAs exist in the cell type and, more importantly, whether the lncRNA is correctly transported to and located at its site of action. Therefore, the deregulation of RBPs in cancer has a profound impact on the associated lncRNAs because it affects the localization and in turn affects their function. Interestingly, drug sensitivity analysis and molecular docking analysis of a dysregulated RBP, *NSUN6*, in the TNBC cell line found that it is associated with sensitivity to the drug navitoclax. Previous studies have demonstrated that navitoclax can target epidermal growth factor receptor (*EGFR*) in TNBC [37]. Our results showed that *NSUN6* may be a target of navitoclax. *NSUN6* is associated with *WAC-AS1*, which are both oncogenes. Based on this, we speculated that inhibiting these RBPs may affect the subcellular localization of lncRNA or even affect its function. However, additional experiments are required to validate these hypotheses. It is worth noting that the experimental verification of lncRNA-protein interactions is still time-consuming and expensive, which is the main technical bottleneck in the field of lncRNA-protein interactions.

The most significant contribution of this research was demonstrating the relationship between the RBPLSig and TIME. Some studies indicate that manipulating the level of citrate can affect the behaviors of both cancer and immune cells, resulting in the induction of cancer cell apoptosis, boosting immune responses, and enhancing cancer immunotherapy [38–43]. The complex interplay between tumor cells and TIME not only plays a pivotal role during tumor development but also has significant effects on immunotherapeutic efficacy and patient OS [44]. Furthermore, CD8 T cell infiltration has been reported to be associated with better OS in BRCA patients [45,46]. Our results showed that the score of immune cell infiltration in the low-risk group was higher, whereas the expression of CD8 T cells and memory-activated CD4 T cells in the low-risk group was higher, indicating that the infiltration of specific immune cells could expedite tumor progression and predict BRCA survival rates. Meanwhile, immune checkpoint blockade therapies have been proposed as a promising approach to treat a variety of malignancies. The increased expression level of immune checkpoint ligands and tumor-associated antigens on tumor cells is correlated with good ICI treatment outcomes [47]. Notably, when detecting ICIs, we found that the risk score was associated with the expression of ICIs. *CTLA-4*, *PD-1*, and *PD-L1* were highly expressed in the low-risk group, indicating that patients with low-risk scores might benefit more from anti-*CTLA-4*, *PD-*

1, and *PD-L1* immunotherapy. As a novel antitumor target comparable to *PD-L1*, *Siglec-15* has also been implicated in immune tolerance regulation and might play an essential role in autoimmune and auto-inflammatory diseases and tumorigenesis [48]. For patients who do not respond to *PD-1*/*PD-L1* antibodies, targeting *Siglec-15* could be an effective alternative therapy. Patients with high-risk scores might also benefit more from anti-*Siglec-15* immunotherapy, which provides new insights into BRCA immunotherapy.

As a highly heterogeneous tumor, BRCA has four distinct molecular subtypes that are more important for survival prognosis and guide individual therapeutic decisions [49,50]. Generally, TNBCs in young patients are much larger than those in the elderly, and therefore, the former might prove to be an appropriate cohort for cancer immunotherapy. Our studies illustrated that the low-risk score appeared to be maintained in patients with luminal A and TNBC. To provide an individualized and accurate prediction, a nomogram for BRCA subtype patients (luminal A and TNBC) that was appropriate for immunotherapy evaluation was constructed. Results of the calibration curve demonstrate that it performed well.

5. Conclusions

In summary, the RBPLSig could provide promising evidence for OS prediction. Furthermore, the RBPLSig is associated with immune infiltration levels and could be a new biomarker to predict the therapeutic response of the BRCA patient. However, further studies are necessary to evaluate the accuracy of our nomogram and prediction online tools for patients with different breast cancer subtypes. More experiments are also necessary to confirm the potential role of RBP-related lncRNAs.

Availability of Data and Materials

The datasets analyzed during the current study are available in the TCGA repository (https://tcga-data.nci.nih.gov/tcga/) and GEO repository (https://www.ncbi.nlm.nih.gov/geo/).

Author Contributions

QX, JZ and HZ conceived and designed the study. JZ and HZ analyzed and interpreted the data. YG, KH, QD, and WS verified the data. JZ associated all the statistical analysis. QX, HZ, and JZ prepared figures and wrote the manuscript. All authors have read and approved the final version.

Ethics Approval and Consent to Participate

Not applicable.

Acknowledgment

Not applicable.

Funding

The present study was supported by the Natural Science Foundation of China (#81701185), the High School Key Research Project of Henan Province (#22A320039), and the ZHONGYUAN QIANREN JIHUA (#ZYQR20191205).

Conflict of Interest

HZ is an employee of Zhengzhou Revogene Ltd. QX was an employee of Zhengzhou Revogene Ltd at the time this research was conducted. All authors declare that they have no conflict of interest.

Supplementary Material

Supplementary material associated with this article can be found, in the online version, at https://doi.org/10.31083/j.fbl2801009.

References

[1] Harbeck N, Penault-Llorca F, Cortes J, Gnant M, Houssami N, Poortmans P, *et al*. Breast cancer. Nature Reviews Disease Primers. 2019; 5: 66.

[2] Pashayan N, Antoniou AC, Ivanus U, Esserman LJ, Easton DF, French D, *et al*. Personalized early detection and prevention of breast cancer: ENVISION consensus statement. Nature Reviews Clinical Oncology. 2020; 17: 687–705.

[3] Nagini S. Breast Cancer: Current Molecular Therapeutic Targets and New Players. Anti-Cancer Agents in Medicinal Chemistry. 2017; 17: 152–163.

[4] Klinge CM. Non-Coding RNAs in Breast Cancer: Intracellular and Intercellular Communication. Noncoding RNA. 2018; 4: 40.

[5] Volovat SR, Volovat C, Hordila I, Hordila DA, Mirestean CC, Miron OT, *et al*. MiRNA and LncRNA as Potential Biomarkers in Triple-Negative Breast Cancer: A Review. Frontiers in Oncology. 2020; 10: 526850.

[6] Fernández-Rojas MA, Melendez-Zajgla J, Lagunas VM. LincRNA-RP11400K9.4 Regulates Cell Survival and Migration of Breast Cancer Cells. Cancer Genomics - Proteomics. 2020; 17: 769–779.

[7] Shi Q, Li Y, Li S, Jin L, Lai H, Wu Y, *et al*. LncRNA DILA1 inhibits Cyclin D1 degradation and contributes to tamoxifen resistance in breast cancer. Nature Communications. 2020; 11: 5513.

[8] Wu Z, Liu Y, Wei L, Han M. LncRNA OIP5-as1 Promotes Breast Cancer Progression by Regulating miR-216a-5p/GLO1. Journal of Surgical Research. 2021; 257: 501–510.

[9] Gerstberger S, Hafner M, Tuschl T. A census of human RNA-binding proteins. Nature Reviews Genetics. 2014; 15: 829–845.

[10] Lv Q, Dong F, Zhou Y, Cai Z, Wang G. RNA-binding protein SORBS2 suppresses clear cell renal cell carcinoma metastasis by enhancing MTUS1 mRNA stability. Cell Death & Disease. 2020; 11: 1056.

[11] Wang Z, Li B, Luo Y, Lin Q, Liu S, Zhang X, *et al*. Comprehensive Genomic Characterization of RNA-Binding Proteins across Human Cancers. Cell Reports. 2018; 22: 286–298.

[12] Chen L. Linking Long Noncoding RNA Localization and Function. Trends in Biochemical Sciences. 2016; 41: 761–772.

[13] Chai Y, Liu J, Zhang Z, Liu L. HuR-regulated lncRNA NEAT1 stability in tumorigenesis and progression of ovarian cancer. Cancer Medicine. 2016; 5: 1588–1598.

[14] Hu Y, Jin Y, Wu X, Yang Y, Li Y, Li H, *et al*. LncRNA-

HGBC stabilized by HuR promotes gallbladder cancer progression by regulating miR-502-3p/SET/AKT axis. Molecular Cancer. 2019; 18: 167.
[15] Yoon J, Abdelmohsen K, Kim J, Yang X, Martindale JL, Tominaga-Yamanaka K, *et al*. Scaffold function of long non-coding RNA HOTAIR in protein ubiquitination. Nature Communications. 2013; 4: 2939.
[16] Noh JH, Kim KM, Abdelmohsen K, Yoon JH, Panda AC, Munk R, *et al*. HuR and GRSF1 modulate the nuclear export and mitochondrial localization of the lncRNA RMRP. Genes & Development. 2016; 30: 1224–1239.
[17] Ferris RL, Blumenschein G, Fayette J, Guigay J, Colevas AD, Licitra L, *et al*. Nivolumab for Recurrent Squamous-Cell Carcinoma of the Head and Neck. New England Journal of Medicine. 2016; 375: 1856–1867.
[18] Schober P, Boer C, Schwarte LA. Correlation Coefficients: Appropriate Use and Interpretation. Anesthesia & Analgesia. 2018; 126: 1763–1768.
[19] Subramanian A, Tamayo P, Mootha VK, Mukherjee S, Ebert BL, Gillette MA, *et al*. Gene set enrichment analysis: a knowledge-based approach for interpreting genome-wide expression profiles. Proceedings of the National Academy of Sciences of the United States of America. 2005; 102: 15545–15550.
[20] Liberzon A, Birger C, Thorvaldsdottir H, Ghandi M, Mesirov JP, Tamayo P. The Molecular Signatures Database (MSigDB) hallmark gene set collection. Cell Systems. 2015; 1: 417–425.
[21] Zhou J, Guo Y, Huo Z, Xing Y, Fang J, Ma G, *et al*. Identification of therapeutic targets and prognostic biomarkers from the hnRNP family in invasive breast carcinoma. Aging. 2021; 13: 4503–4521.
[22] Xu Q, Deng F, Xing Z, Wu Z, Cen B, Xu S, *et al*. Long non-coding RNA C2dat1 regulates CaMKIIdelta expression to promote neuronal survival through the NF-kappaB signaling pathway following cerebral ischemia. Cell Death and Disease. 2016; 7: e2173.
[23] Hess B, Kutzner C, van der Spoel D, Lindahl E. GROMACS 4: Algorithms for Highly Efficient, Load-Balanced, and Scalable Molecular Simulation. Journal of Chemical Theory and Computation. 2008; 4: 435–447.
[24] Bolha L, Ravnik-Glavač M, Glavač D. Long Noncoding RNAs as Biomarkers in Cancer. Disease Markers. 2017; 2017: 7243968.
[25] Meng L, Ward AJ, Chun S, Bennett CF, Beaudet AL, Rigo F. Towards a therapy for Angelman syndrome by targeting a long non-coding RNA. Nature. 2015; 518: 409–412.
[26] Slack FJ, Chinnaiyan AM. The Role of Non-coding RNAs in Oncology. Cell. 2019; 179: 1033–1055.
[27] Jonas K, Calin GA, Pichler M. RNA-Binding Proteins as Important Regulators of Long Non-Coding RNAs in Cancer. International Journal of Molecular Sciences. 2020; 21: 2969.
[28] Wang D, Li J, Cai F, Xu Z, Li L, Zhu H, *et al*. Overexpression of MAPT-as1 is associated with better patient survival in breast cancer. Biochemistry and Cell Biology. 2019; 97: 158–164.
[29] Yang H, Yang W, Dai W, Ma Y, Zhang G. LINC00667 promotes the proliferation, migration, and pathological angiogenesis in non-small cell lung cancer through stabilizing VEGFA by EIF4a3. Cell Biology International. 2020; 44: 1671–1680.
[30] Yu J, Wang F, Zhang J, Li J, Chen X, Han G. LINC00667/miR-449b-5p/YY1 axis promotes cell proliferation and migration in colorectal cancer. Cancer Cell International. 2020; 20: 322.
[31] Zhong Y, Li Y, Song T, Zhang D. MiR-718 mediates the indirect interaction between lncRNA SEMA3B-as1 and PTEN to regulate the proliferation of hepatocellular carcinoma cells. Physiological Genomics. 2019; 51: 500–505.
[32] Guo W, Liang X, Liu L, Guo Y, Shen S, Liang J, *et al*. MiR-6872 host gene SEMA3B and its antisense lncRNA SEMA3B-as1 function synergistically to suppress gastric cardia adenocarcinoma progression. Gastric Cancer. 2019; 22: 705–722.
[33] Li X, Jin F, Li Y. A novel autophagy-related lncRNA prognostic risk model for breast cancer. Journal of Cellular and Molecular Medicine. 2021; 25: 4–14.
[34] Fan C, Ma L, Liu N. Systematic analysis of lncRNA–miRNA–mRNA competing endogenous RNA network identifies four-lncRNA signature as a prognostic biomarker for breast cancer. Journal of Translational Medicine. 2018; 16: 264.
[35] Li X, Li Y, Yu X, Jin F. Identification and validation of stemness-related lncRNA prognostic signature for breast cancer. Journal of Translational Medicine. 2020; 18: 331.
[36] Sun Z, Jing C, Xiao C, Li T. An autophagy-related long non-coding RNA prognostic signature accurately predicts survival outcomes in bladder urothelial carcinoma patients. Aging. 2020; 12: 15624–15637.
[37] Marczyk M, Patwardhan GA, Zhao J, Qu R, Li X, Wali VB, *et al*. Multi-Omics Investigation of Innate Navitoclax Resistance in Triple-Negative Breast Cancer Cells. Cancers. 2020; 12: 2551.
[38] Huang L, Wang C, Xu H, Peng G. Targeting citrate as a novel therapeutic strategy in cancer treatment. Biochimica et Biophysica Acta (BBA) - Reviews on Cancer. 2020; 1873: 188332.
[39] Ren J, Seth P, Ye H, Guo K, Hanai J, Husain Z, *et al*. Citrate Suppresses Tumor Growth in Multiple Models through Inhibition of Glycolysis, the Tricarboxylic Acid Cycle and the IGF-1R Pathway. Scientific Reports. 2017; 7: 4537.
[40] Colak S, Ten Dijke P. Targeting TGF-beta Signaling in Cancer. Trends in Cancer. 2017; 3: 56–71.
[41] Li H, Zhao W, Shi Y, Li Y, Zhang L, Zhang H, *et al*. Retinoic acid amide inhibits JAK/STAT pathway in lung cancer which leads to apoptosis. Tumor Biology. 2015; 36: 8671–8678.
[42] Macha MA, Rachagani S, Gupta S, Pai P, Ponnusamy MP, Batra SK, *et al*. Guggulsterone decreases proliferation and metastatic behavior of pancreatic cancer cells by modulating JAK/STAT and Src/FAK signaling. Cancer Letters. 2013; 341: 166–177.
[43] Yu H, Jove R. The STATs of cancer — new molecular targets come of age. Nature Reviews Cancer. 2004; 4: 97–105.
[44] Jang N, Kwon HJ, Park MH, Kang SH, Bae YK. Prognostic Value of Tumor-Infiltrating Lymphocyte Density Assessed Using a Standardized Method Based on Molecular Subtypes and Adjuvant Chemotherapy in Invasive Breast Cancer. Annals of Surgical Oncology. 2018; 25: 937–946.
[45] Pantelidou C, Sonzogni O, De Oliveria Taveira M, Mehta AK, Kothari A, Wang D, *et al*. PARP Inhibitor Efficacy Depends on CD8+ T-cell Recruitment via Intratumoral STING Pathway Activation in BRCA-Deficient Models of Triple-Negative Breast Cancer. Cancer Discovery. 2019; 9: 722–737.
[46] Wang Z, Yang X, Shen J, Xu J, Pan M, Liu J, *et al*. Gene expression patterns associated with tumor-infiltrating CD4+ and CD8+ T cells in invasive breast carcinomas. Human Immunology. 2021; 82: 279–287.
[47] Yang Y. Cancer immunotherapy: harnessing the immune system to battle cancer. Journal of Clinical Investigation. 2015; 125: 3335–3337.
[48] van de Wall S, Santegoets KCM, van Houtum EJH, Büll C, Adema GJ. Sialoglycans and Siglecs can Shape the Tumor Immune Microenvironment. Trends in Immunology. 2020; 41: 274–285.
[49] Perou CM, Sørlie T, Eisen MB, van de Rijn M, Jeffrey SS, Rees CA, *et al*. Molecular portraits of human breast tumours. Nature. 2000; 406: 747–752.
[50] Yeo SK, Guan JL. Breast Cancer: Multiple Subtypes within a Tumor? Trends in Cancer. 2017; 3: 753–760.